Dynamics of Magnus-dominated particle clusters, collisions, pinning, and ratchets

C. Reichhardt and C. J. O. Reichhardt

Theoretical Division and Center for Nonlinear Studies, Los Alamos National Laboratory, Los Alamos, New Mexico 87545, USA

(Received 21 February 2020; accepted 19 May 2020; published 3 June 2020)

Motivated by the recent work in skyrmions and active chiral matter systems, we examine pairs and small clusters of repulsively interacting point particles in the limit where the dynamics is dominated by the Magnus force. We find that particles with the same Magnus force can form stable pairs, triples, and higher ordered clusters or exhibit chaotic motion. For mixtures of particles with opposite Magnus force, particle pairs can combine to form translating dipoles. Under an applied drive, particles with the same Magnus force translate; however, particles with different or opposite Magnus force exhibit a drive-dependent decoupling transition. When the particles interact with a repulsive obstacle, they can form localized orbits with depinning or unwinding transitions under an applied drive. We examine the interaction of these particles with clusters or lines of obstacles and find that the particles can become trapped in orbits that encircle multiple obstacles. Under an ac drive, we observe a series of ratchet effects, including ratchet reversals, for particles interacting with a line of obstacles due to the formation of commensurate orbits. Finally, in assemblies of particles with mixed Magnus forces of the same sign, we find that the particles with the largest Magnus force become localized in the center of the cluster, while for mixtures with opposite Magnus forces, the motion is dominated by transient local pairs or clusters, where the translating pairs can be regarded as a form of active matter.

DOI: 10.1103/PhysRevE.101.062602

I. INTRODUCTION

A variety of systems can be described as local clusters of interacting particles, including colloids [1–3], Coulomb clusters [4,5], vortices in type II superconductors [6,7], dusty plasmas [8], Wigner crystals [9], vortices in superfluids [10,11], skyrmions [12,13], granular matter [14], and active matter assemblies [15]. In many of these systems, the cluster formation arises when the particles experience a local confinement or self-trapping due to the nature of the pairwise particle-particle interactions [16,17]. Under various types of driving, these systems can exhibit interesting dynamical effects, including self-assembly [18,19], rotating gear behavior [20,21], and depinning phenomena [22]. In most of these systems, the dynamics is overdamped; however, some systems also include nondissipative effects such as inertia or Magnus forces. In particular, Magnus forces produce a velocity component that is perpendicular to the net force experienced by a particle, and such forces arise for vortices in fluids [23–26], active spinners [27–31], chiral active matter [32], charged particles in magnetic fields [33], and skyrmions in chiral magnets [34–36]. One consequence of this is that pairs or clusters of particles can undergo rotations or spiraling motion when they enter a confining potential [37–41] or are subjected to a quench [42]. If damping is present, these spiraling motions are transient unless there is some form of external driving. Less is known about how Magnus-dominated particles would interact with obstacles or pinning sites; however, some studies indicate that the Magnus force strongly modifies the dynamics compared to overdamped systems [40–49].

Motived by our previous work on point particle models of skyrmions interacting with each other and with random [41,50] or periodic pinning [42], where the particles have both a Magnus and a damping force, we consider the limits of zero damping or very low damping and study the Magnus-dominated dynamics of pairs and small clusters of particles interacting with each other and with pinning sites. We consider mixtures with identical Magnus forces, dispersion in the Magnus force, and assemblies with opposite Magnus forces.

The paper is organized as follows. We describe our simulation model in Sec. II. In Sec. III we consider a pair of particles with the same sign and strength of the Magnus force. We find that a bound rotating pair forms despite the repulsive particle-particle interactions, and in Sec. III A we show that a pair with equal strength but opposite sign of the Magnus force forms a dipole which translates in a direction determined by the initial orientation of the pair, with dipoles of smaller size translating more rapidly. When we add an external drive as in Sec. IV, particle pairs with equal Magnus force remain coupled and translate at 90° with respect to the driving direction, while pairs with opposite Magnus force sign undergo a drive-dependent decoupling transition. In Sec. IV A, when repulsive obstacles are added to the system, individual or clustered particles can form stable bound circulating orbits around the obstacles and exhibit a depinning transition under an applied drive. If damping is present, the pinned states are transient and the particle or particles gradually spiral away from the obstacle. As shown in Sec. IV B, an asymmetric cluster of defects produces a diode-like effect for driving in different directions in the overdamped limit, but in the Magnus-dominated limit this diode effect disappears and the particles circle around the entire cluster. A particle driven toward a line of obstacles experiences a Magnus force-induced deviation in its direction of motion as it approaches the line until it breaks through the line, and this deviation is reduced for increased driving force. We also find

that it is possible to produce a ratchet effect for a particle that is placed by a line of obstacles when a biharmonic ac drive is applied. Here the particle can form circular orbits that create a gearlike motion when combined with the periodicity of the line of obstacles. Reversals in the ratchet current occur as a function of ac amplitude and Magnus force. In Sec. IV C, for clusters of more than two particles we find various types of stable rotating states, including rotating pairs that encircle each either. For larger clusters we observe chaotic dynamics in which the system breaks up into smaller clusters with some particles jumping from one cluster to another. When the Magnus force varies strongly among the particles in the cluster, as in Sec. IV D, the motion is chaotic and the particles with the largest Magnus forces become localized in the center of the cluster. Section IV E describes the cluster collisions that occur when the Magnus forces are of different sign and strength. Particles can form translating pairs that break apart and re-form if a collision with an obstacle or other particles occurs. We argue that assemblies of particles with mixed Magnus force sign represent a new example of an active matter system. In Sec. V we discuss implications of our system for skyrmion or meron motion as well as connections to studies of point vortex models. A summary of the results appears in Sec. VI.

Our results should be relevant for skyrmions in the absence of damping or in the low damping limit in the presence of a drive, for certain models of point vortex dynamics in superfluids or Bose-Einstein condensates with fluid flows, and for active spinners and active chiral colloidal systems.

II. SIMULATION

We consider a two-dimensional system with periodic boundary conditions in the x and y directions containing N particles that are initially placed at fixed distances from each other. Typically we use initial conditions in which the particles are in one-dimensional lines. The dynamics of particle i are governed by the following undamped equation of motion:

$$\alpha_m^i \hat{z} \times \mathbf{v}_i = \mathbf{F}_i^{pp} + \mathbf{F}^{obs} + \mathbf{F}^D, \tag{1}$$

where $\mathbf{v}_i$ is the velocity of particle i and α_m^i is the coefficient of the Magnus term, which creates a velocity component perpendicular to the net applied forces. Each particle can be assigned a different amplitude or sign of α_m^i. The particle-particle interaction force is given by $\mathbf{F}_i^{pp} = \sum_{j=1}^{N} K_1(r_{ij})\hat{\mathbf{r}}_{ij}$, where $r_{ij} = |\mathbf{r}_i - \mathbf{r}_j|$ is the distance between particles i and j, $\hat{\mathbf{r}}_{ij} = (\mathbf{r}_i - \mathbf{r}_j)/r_{ij}$, and the modified Bessel function $K_1(r)$ falls off exponentially for large r. This form of the interaction was previously used in particle-based models of skyrmions in two-dimensional systems [40–42,50]. The driving force $\mathbf{F}^D = F^D\hat{\mathbf{x}}$ is applied uniformly to all particles. An individual particle in the Magnus force-dominated limit moves at 90° with respect to the driving force, so that when the drive is applied in the x direction, the particle moves in the y direction. The term $\mathbf{F}^{obs} = \sum_{k=1}^{N_p}$ represents the force from N_p obstacles, which take the form of particles that are permanently fixed in place. In some cases, we add a damping term $\alpha_d^i \mathbf{v}_i$ to the equation of motion which aligns the velocities in the direction of the external forces. Under a drive, a particle experiencing both Magnus and damping forces moves at an angle $\theta = \arctan(\alpha_m/\alpha_d)$. We measure the particle velocities both parallel, $\langle V_x \rangle = N^{-1}\sum_i^N \mathbf{v}_i \cdot \hat{\mathbf{x}}$, and perpendicular, $\langle V_y \rangle = N^{-1}\sum_i^N \mathbf{v}_i \cdot \hat{\mathbf{y}}$, to the drive.

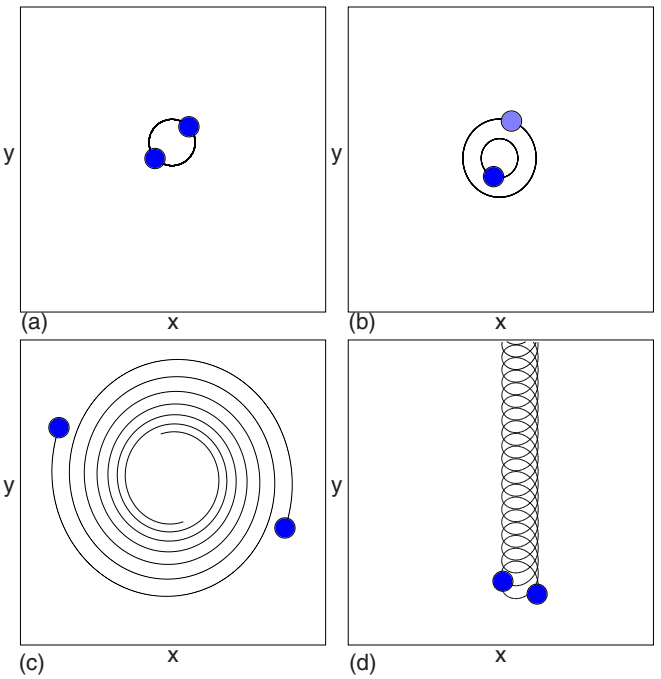

FIG. 1. The particle locations (dots) and trajectories (lines) for pairs of interacting particles. (a) When $\alpha_m^1 = \alpha_m^2 = 1.0$, the particles form a clockwise rotating bound pair. (b) For $\alpha_m^1 = 2.0$ and $\alpha_m^2 = 1.0$, the particles form nested orbits where the particle with the higher Magnus force is closer to the center. (c) A system with $\alpha_m^1 = \alpha_m^2 = 1.0$ in which a finite damping term $\alpha_d = 0.1$ has also been added, causing the particles to spiral out gradually. (d) The $\alpha_m^1 = \alpha_m^2 = 1.0$ system from (a) with an additional drift force $F_D = 0.075$ applied in the x direction, causing the pair to translate in the negative y direction.

III. DYNAMICS OF COUPLED PARTICLES

We first consider particles with the same sign and strength of the Magnus force. In Fig. 1(a) we show an image of the trajectories of two particles with $\alpha_m^1 = \alpha_m^2 = 1.0$ initialized a distance R apart. In an overdamped system, the particles would move away from each other, but here they form a pair and rotate around each other in a clockwise manner. The particles remain confined to the pair due to the Magnus force, which generates velocities that are perpendicular to the net forces on each particle. When $\alpha_m^1 \neq \alpha_m^2$, the particles form a nested pair as illustrated in Fig. 1(b) for $\alpha_m^1 = 1.0$ and $\alpha_m^2 = 2.0$, with the larger Magnus force particle orbiting closer to the center. If we add a finite damping term of $\alpha_d = 0.1$ to the $\alpha_m^1 = \alpha_m^2 = 1.0$ system in Fig. 1(a), the particles gradually spiral away from each other as shown in Fig. 1(c), and in the long time limit, the presence of damping eventually causes the particles to come to a standstill. If only one particle has damping, the overall motion still damps away since the damped particle couples to the undamped particle and dissipates its energy, and so as long as there is some damping in the system

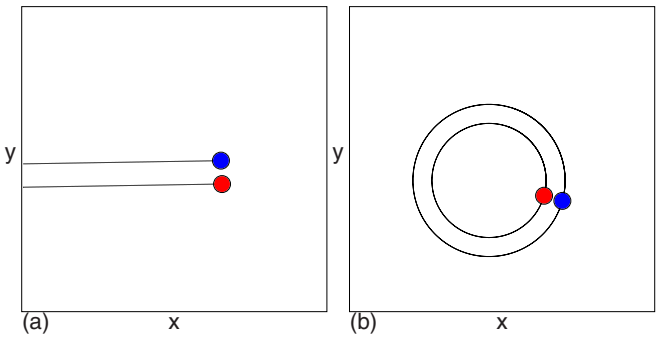

FIG. 2. The particle locations (dots) and trajectories (lines) for pairs of interacting particles. (a) When $\alpha_m^1 = 2.0$ and $\alpha_m^2 = -2.0$, the particles form a dipole that translates in a fixed direction. (b) When $\alpha_m^1 = 1.65$ and $\alpha_m^2 = -2.0$, the dipole moves in a circular orbit.

both particles will eventually come to rest unless an external drive is applied. In the zero damping limit, when there is an applied drive the rotating pair remains coupled and its center of mass translates, as shown in Fig. 1(c) for the $\alpha_m^1 = \alpha_m^2 = 1.0$ system under a drive of $F_D = 0.075$. The x direction drive causes the pair to translate in the negative y direction, giving a skyrmion Hall angle of 90°. Here the intrinsic skyrmion Hall angle is defined as $\theta_{sk}^{\rm int} = \arctan(\alpha_m/\alpha_d)$ [41,43,46]. In the presence of damping, the driven pair in Fig. 1(d) gradually spiral away from each other and translate separately at a Hall angle less than 90°.

A. Systems with opposite Magnus force

When two particles that have Magnus forces which are equal in strength but opposite in sign are brought together, they form a bound pair that translates in a fixed direction even in the absence of an applied drive. The repulsive interaction between the two particles produces an outwardly directed force on each particle, and the Magnus term rotates this force by 90° for one particle and by −90° for the other, producing a net translation instead of a rotation. In Fig. 2(a) a pair of particles with $\alpha_m^1 = 2.0$ and $\alpha_m^2 = -2.0$ maintain a fixed distance from each other and translate in a direction that is determined by the initial placement of the particles. The speed of the dipole pair increases as the initial distance R between the particles decreases, since the pairwise interaction force increases at smaller distances, while the dipole drift velocity V_d is given by $V_d \propto K_1(R)/\alpha_m$, where $\alpha_m = |\alpha_m^1| = |\alpha_m^2|$. In Fig. 3(a) we plot the measured velocity V_d versus α_m for the system in Fig. 2(a) at a fixed initial separation distance of $R = 2.0$. The solid line indicates $1/\alpha_m$ behavior. In Fig. 3(b) we show V_d versus R for fixed $\alpha_m = 1.0$ in the same system. The dipole velocity decreases approximately exponentially with increasing distance at large R, as expected for the function $K_1(R)$. In Fig. 2(b) we illustrate the dipole trajectory for a system with Magnus forces of opposite sign but unequal strength, $\alpha_m^1 = 1.65$ and $\alpha^2 = -2.0$, where the dipole curves into a localized circular orbit. As the difference in strength of the Magnus forces increases, the circular orbit becomes tighter.

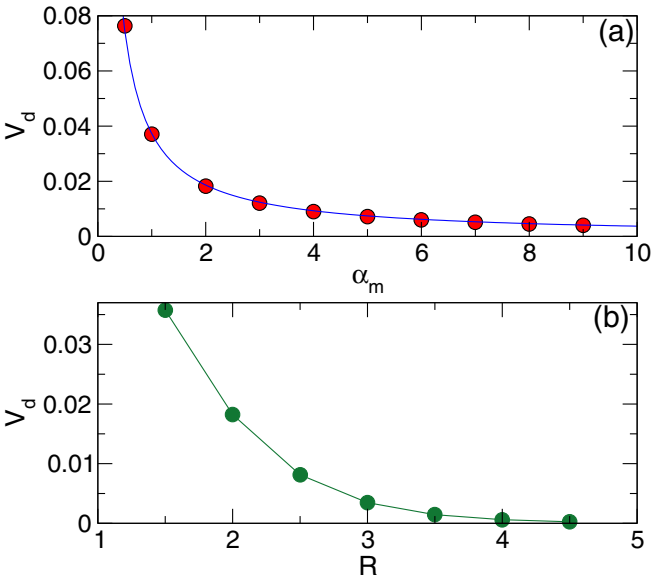

FIG. 3. Dots: The measured dipole velocity V_d vs α_m for the system in Fig. 2(a) with $\alpha_m^1 = \alpha_m$ and $\alpha_m^2 = -\alpha_m$, where the initial distance between the particles is $R = 2.0$. The solid blue line indicates $1/\alpha_m$ behavior. (b) V_d vs R for the same system with fixed $\alpha_m = 2.0$.

IV. DYNAMICS UNDER A DRIVE

We next consider the effect of applying a driving force in the positive x direction, which causes isolated particles with a positive Magnus force to move in the negative y direction. For a pair of particles with Magnus forces of equal sign and strength, the pair remains coupled when the drive is applied and translates perpendicular to the drive, as shown in Fig. 1(d). If the strengths of the Magnus forces are unequal, there is a critical driving force above which the pair decouples. In Fig. 4 we plot the velocities V_1 and V_2 of a pair of particles versus driving force F_D for a system with $\alpha_m^1 = 1.6$ and $\alpha_m^2 = 2.0$. For $F_D \leqslant 0.15$, $V_1 = V_2$ and the particles are coupled into a

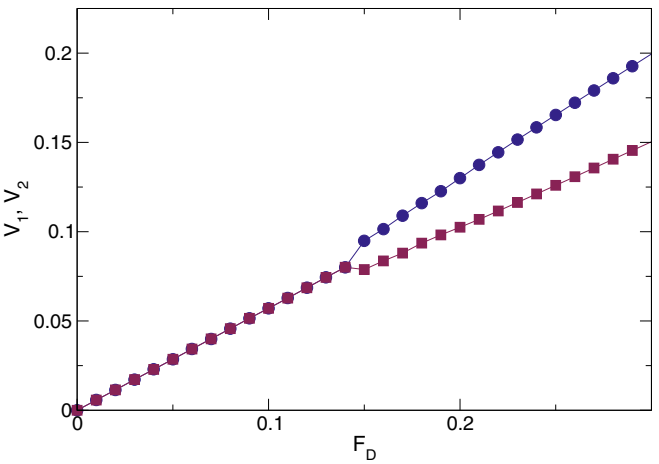

FIG. 4. The velocities V_1 (blue) and V_2 (red) of a pair of particles vs F_D for a system with $\alpha_m^1 = 1.6$ and $\alpha_m^2 = 2.0$, showing a drive-induced decoupling transition near $F_D = 0.15$.

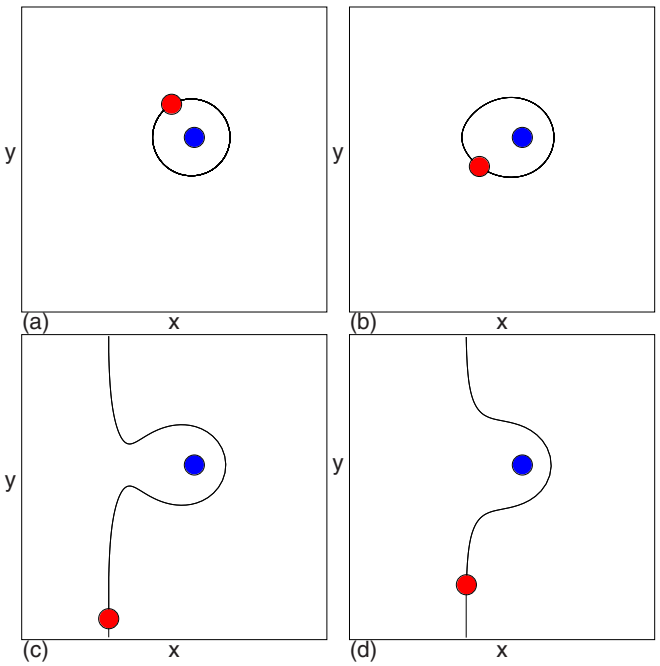

FIG. 5. The particle position (red dot) and trajectory (line) with the obstacle location (blue dot) for a single particle interacting with a stationary obstacle in the form of a permanently fixed particle. The particle has $\alpha_m = 2.0$ and is initialized at a distance $R = 1.5$ from the obstacle, and the applied drive is (a) $F_D = 0.005$, (b) $F_D = 0.015$, (c) $F_D = 0.0165$, and (d) $F_D = 0.025$.

dipole, while for $F_D > 0.15$, the pair decouples as indicated by the change in the velocities. The critical driving force F_c at which the decoupling occurs decreases as the difference $|\alpha_m^1 - \alpha_m^2|$ increases, while F_c increases as the separation R decreases.

A cluster containing more than two particles that all have the same α_m remains coupled under an applied drive, but when some of the particles have different values of α_m, multiple decoupling transitions can occur.

A. Dynamics with obstacles and depinning

We next study the effects of driven particles interacting with a repulsive obstacle. To begin, we consider a single particle under an applied drive interacting with an obstacle which is modeled as another particle that is fixed permanently in place, giving a repulsive force between the particle and the obstacle. In the overdamped limit, there is no pinning effect and the particle simply moves away from the obstacle due to the pairwise repulsion. In Fig. 5(a), a particle with $\alpha_m = 2.0$ under a driving force of $F_D = 0.005$ initialized at a distance of $R = 1.5$ from the obstacle forms a localized pinned orbit around the obstacle. At $F_D = 0.015$ in the same system, Fig. 5(b) indicates that the particle is still localized but the orbit becomes distorted by the drive. In Fig. 5(c) at $F_D = 0.165$, the particle has depinned and translates in the y direction, interacting with the obstacle during each pass through the periodic boundary conditions. At $F_D = 0.025$ in Fig. 5(d), the interaction with the obstacle is diminished, and the pinch point in the trajectory near the obstacle has

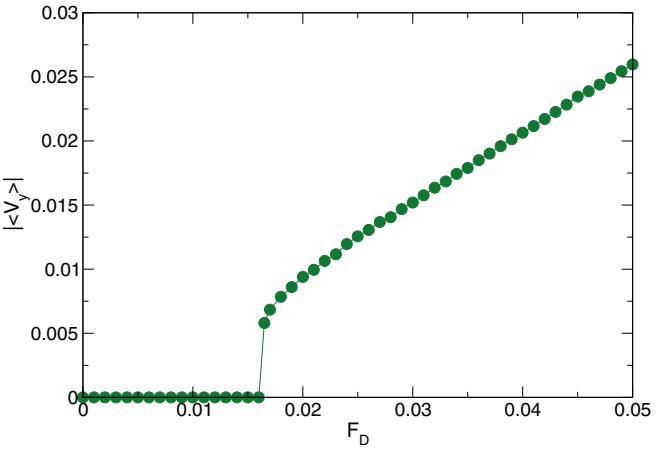

FIG. 6. $|\langle V_y \rangle|$, the absolute value of the average velocity in the y direction of the particle from the system in Fig. 5, vs F_D, showing a depinning transition at $F_D = 0.016$.

disappeared. Phase portraits of the evolution of trajectories of this type were previously studied for the case of a point vortex interacting with a stationary obstacle [51–54]. In Fig. 6(a) we plot the absolute value of the average particle velocity in the y direction, $|\langle V_y \rangle|$, versus F_D. We find a clear region where the particle is pinned, as indicated by $|\langle V_y \rangle| = 0$, along with a critical depinning force at $F_c = 0.016$. In most systems where depinning occurs, there must be an attractive interaction between the particle and a defect so that the particle can settle into a potential energy minimum and stop moving. It is possible in some overdamped systems for the particle to become trapped behind a repulsive barrier, but even in that case the particle comes to rest and can be described as jammed [22]. Here we find a depinning transition in which the particle is always moving but remains localized below depinning. If the sign of the Magnus force is reversed, the same dynamics occurs but the particle depins in the opposite direction. The depinning threshold depends on the strength of α_m and the initial distance R at which the particle is placed from the obstacle.

If we add some damping to the particle dynamics, the particle does not remain localized but always escapes via an unwinding transition. This process is illustrated in Fig. 7(a) for the system from Fig. 5 with an added damping of $\alpha_d = 0.01$ at a fixed drive of $F_D = 0.01$, which is below the threshold depinning force found in Fig. 6 for the undamped system. When damping is present, after each orbit the particle gradually moves away from the obstacle until eventually it depins and then translates at an angle $\theta_{sk} = \arctan(\alpha_m/\alpha_d)$. If the interaction between the particle and the obstacle is attractive, when damping is present the particle gradually spirals into the obstacle, while if a drive is also applied, the particle spirals inward until it reaches an equilibrium point at which the driving force balances the attractive force from the obstacle.

A single repulsive obstacle can also capture multiple particles. An example of this process appears in Fig. 8(a) for a sample with two particles where $\alpha_m^1 = \alpha_m^2 = 2.0$, $R = 1.5$, and $F_D = 0.005$, where the two particles form a pair that rotates around the obstacle. Due to the applied drive, the trajectories are denser on the left side of the obstacle. When the

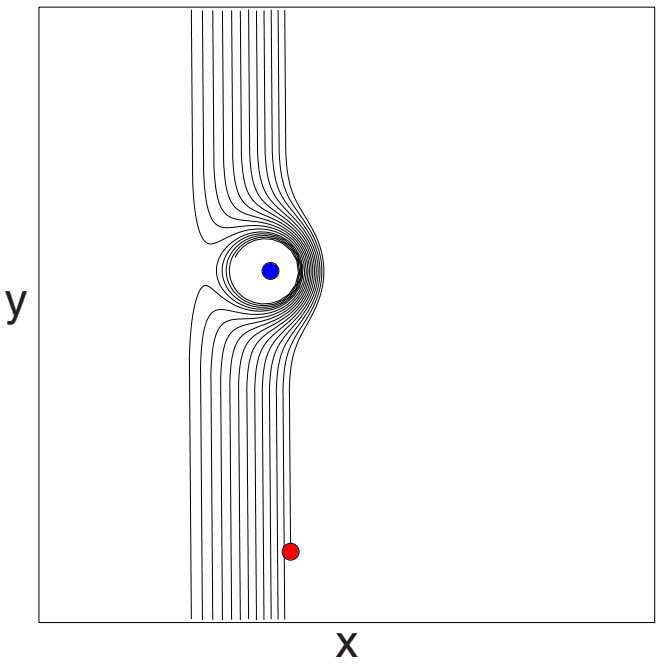

FIG. 7. The particle position (red dot) and trajectory (lines) along with the obstacle location (blue dot) for the system from Fig. 5 with $\alpha_m = 2.0$ and $R = 1.5$ at $F_D = 0.01$ where an additional damping term of $\alpha_d = 0.01$ has been added to the dynamics. The particle gradually spirals away from the obstacle.

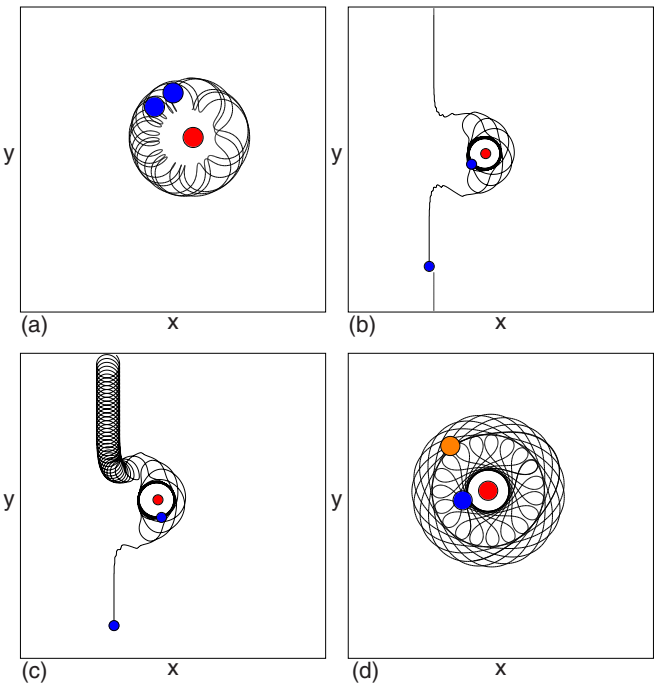

FIG. 8. The particle positions (blue and orange dots) and trajectories (lines) along with the obstacle position (red dot). (a) Two particles trapped at an obstacle for $\alpha_m^1 = \alpha_m^2 = 2.0$ at $F_D = 0.005$ and $R = 1.5$. (b) The same system at $F_D = 0.01$ where only one particle can be trapped. (c) The same system at $F_D = 0.01$ in which the two particles are initially in a rotating pair that collides with the defect, which traps one of the particles. (c) Two particles trapped at an obstacle for $\alpha_m^1 = 2.0$ and $\alpha_m^2 = -2.0$ at $F_D = 0.005$ and $R = 1.5$, where the Magnus forces of the particles have opposite signs.

drive is increased, a depinning transition occurs in which one particle depins while the other remains localized, as shown in Fig. 8(b) for the same system at $F_D = 0.01$. Due to the periodic boundary conditions, the depinned particle returns and interacts with the obstacle again, passing through a spiraling orbit before escaping. At a higher drive of $F_D > 0.015$, the second particle also depins. If the two particles are initially in a pair away from the obstacle, then when they collide with the obstacle under a driving force, the obstacle can trap the pair, only one particle, or neither particle. In Fig. 8(c) we show the collision of a pair with the obstacle at $F_D = 0.01$, where one particle becomes trapped and the other escapes. For $F_D > 0.015$, the pair stays together after encountering the obstacle, while for $F_D < 0.05$, both particles become trapped. If the Magnus force is different in a pair of trapped particles, two orbits form with two different average distances from the obstacle. Even if the two particles have Magnus forces of opposite sign, they can still form a pinned state as shown in Fig. 8(d) for a sample with $\alpha_m^1 = 2.0$, $\alpha_m^2 = -2.0$, $R = 1.5$, and $F^D = 0.005$. Studies of the nonlinear dynamics of a pair of point vortices interacting with an obstacle, where similar effects appear, can be found in Refs. [55–57].

B. Interaction with multiple obstacles and ratchet effects

When multiple obstacles are present, a single particle can move around or encircle a cluster of obstacles to create an edge current effect. In an overdamped system, when particles interact with an asymmetric array of defects, it is possible to create a diode effect in which the depinning threshold is higher in one direction than the other. In Fig. 9(a) we show seven obstacles that have been arranged into a funnel shape. When a mobile particle is initially placed near one of the obstacles, it can encircle a single obstacle or it can encircle all of the obstacles, as shown in Fig. 9(a) for an $\alpha_m = 1.0$ particle placed at a distance of $R = 1.5$ from the funnel, where $F_D = 0.0$. This ability to encircle multiple obstacles indicates that the Magnus-dominated particle exhibits an edge current behavior of the type observed in chiral active matter systems [58,59]. Under application of a drive in the *negative x* direction with $F^D = 0.01$, Fig. 9(a) indicates that the particle moves in the positive y direction and curves around the array of obstacles. The same drive of $F^D = 0.01$ applied in the positive x direction causes the particle to move in the negative y direction, and as shown in Fig. 9(c), the particle skirts around the funnel tip without getting trapped. Under varied parameters, we have not found a case in which the funnel tip is able to trap the particle for driving in any direction. At higher F_D, the particle breaks through the funnel array rather than moving around it, as illustrated in Fig. 9(d) for the system from Fig. 9(c) at $F_D = 0.25$. A nonlinear analysis of the motion of a point vortex through multiple obstacles can be found in Ref. [60].

In Fig. 10(a) we plot the absolute y-direction velocity $|\langle V_y \rangle|$ versus F_D for the system in Fig. 9 for driving in both the positive and negative x directions. There is no pinned regime, and the velocities are almost identical for both directions of

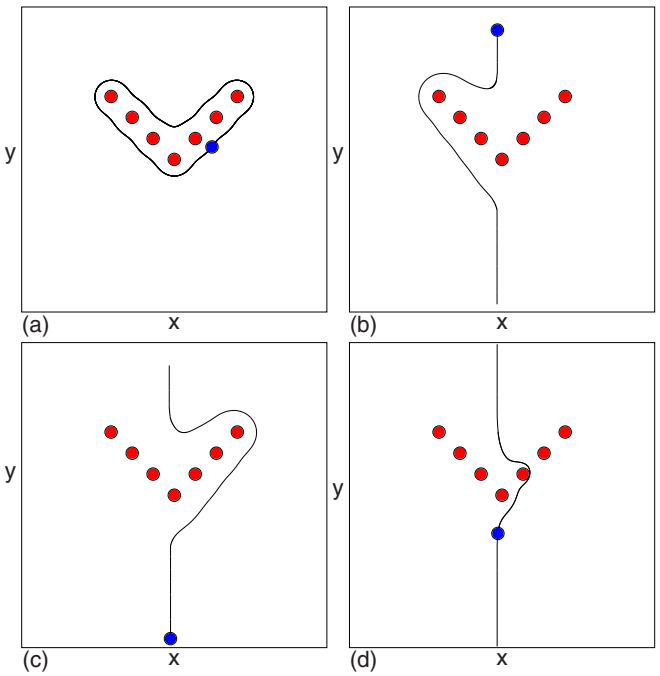

FIG. 9. The particle position (blue dot) and trajectory (line) along with the obstacle positions (red dots) for a particle with $\alpha_m = 1.0$ under a drive interacting with an array of obstacles placed in a funnel configuration. (a) At $F_D = 0.0$, the particle is bound to the funnel array and follows an orbit that encircles the obstacles in a counterclockwise direction. (b) For a *negative* x direction drive of $F_D = 0.01$, the particle moves in the positive y direction and deviates around the obstacles. (c) For a drive of $F_D = 0.01$ applied in the positive x direction, the particle moves in the negative y direction but does not become trapped by the funnel tip. (d) The same as panel (c) at $F_D = 0.250$, where the particle passes through the funnel.

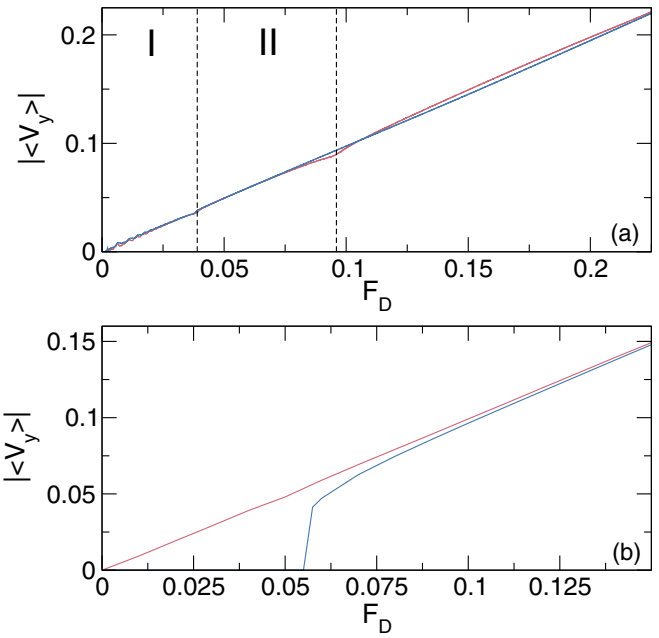

FIG. 10. (a) The absolute velocity $|\langle V_y \rangle|$ vs F_D for the system in Figs. 9(b) and 9(c) for motion in the negative y direction (blue) and positive y direction (pink). For either direction of drive, in Region I, the particle moves around the obstacles, and in Region II, the particle breaks through the funnel between the outer two obstacles. The dashed line at $F_D = 0.95$ indicates a transition for the positive y direction motion to the flow illustrated in Fig. 9(d). Changes in the breakthrough location are associated with small cusps in the velocity-force curve, and additional breakthrough cusps occur at higher drives (not shown). (b) $|\langle V_y \rangle|$ vs F_D for the same system in the overdamped limit of $\alpha_m = 0.0$ and $\alpha_d = 1.0$. There is a finite depinning threshold for motion in the negative y direction (blue) but not for motion in the positive y direction (pink), creating a diode effect.

driving. The label I indicates the regime in which the particle moves around the outer edge of the obstacles as shown in Figs. 9(b) and 9(c), while the label II denotes the regime in which the particle passes between the outer two obstacles. For motion in the positive y direction, the next breakthrough point occurs at $F_D = 0.1$, which appears as a cusp in the velocity, and is associated with a transition to the motion illustrated in Fig. 9(d). This breakthrough transition occurs at a drive higher than the range shown for motion in the negative y direction.

If finite damping is present, we can observe a diode effect which is the most pronounced in the fully overdamped limit. In Fig. 10(b) we plot $|\langle V_y \rangle|$ versus F_D for the system from Fig. 10(a) but with $\alpha_m = 0.0$ and $\alpha_d = 1.0$ under both positive and negative y direction driving. Since the Magnus force is zero, the particle motion is aligned with the driving force direction. There is a finite depinning threshold for motion in the negative y direction, but no threshold for driving in the positive y direction. In Fig. 11(a) we plot the particle trajectory in the overdamped limit of the system in Fig. 10 for a drive of $F^D = 0.04$ in the negative y direction, where the particle becomes trapped by the funnel tip, while in Fig. 11(b) the same system under driving in the positive y direction has continuous flow of the particle around the obstacles.

The appearance of a diode effect in the overdamped system with a funnel array geometry also implies that if an ac drive is applied, a ratchet effect will appear in which the particle translates along the easy flow direction of the funnel during one portion of the ac cycle. This type of ratchet is known as a rocking ratchet [61], and it has been observed in overdamped superconducting vortices interacting with asymmetric pinning [62–66] and in skyrmion systems where there is a combination of damping and a Magnus effect [67,68]. In the skyrmion system there are even cases where a ratchet effect occurs only when the Magnus force is present [67]. The results in Figs. 9 and 10 suggest that if there is only a Magnus force without damping, the ratchet effect is absent, indicating that some damping is necessary for ratcheting to occur; however, we next show that it is still possible to achieve a ratchet effect in the Magnus-dominated regime if the symmetry is broken by a combination of ac driving and the chirality of the Magnus force.

In Fig. 12(a) we plot the trajectory of a particle moving in the negative y direction interacting with a line of obstacles with a period of $a = 1.0$ for a system with $F_D = 0.007$ and $\alpha_m = 2.0$. In the absence of obstacles, the particle moves in a straight line at a constant velocity; however, as the particle approaches the line of obstacles, it begins to bend away from the line due to the repulsive force from the particles in the

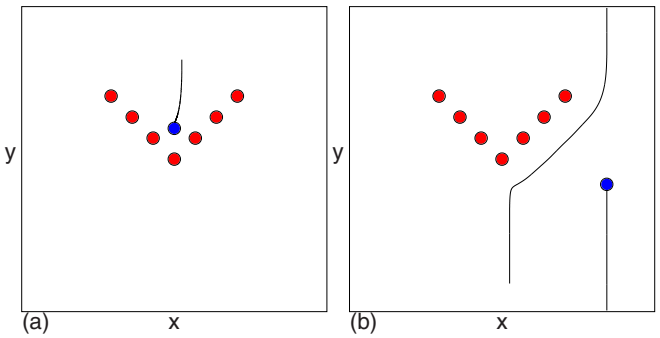

FIG. 11. The particle position (blue dot) and trajectory (line) along with the obstacle positions (red dots) for a particle with $\alpha_m = 0.0$ and $\alpha_d = 1.0$ at $F_D = 0.04$ in the overdamped limit of the system in Fig. 10. (a) Motion in the negative y direction where the particle becomes trapped. (b) Motion in the positive y direction where the particle moves around the obstacle array and does not become trapped.

positive y direction. The Magnus force changes this repulsive force into a positive x direction velocity component of the moving particle. The particle accelerates as it comes closer to the obstacles, and eventually it passes through the barrier. As F_D increases, the particle experiences a smaller x direction deviation of its motion when it approaches the obstacle line, as shown in Fig. 12(b) for $F_D = 0.07$, while for even higher values of F_D, the deviation in the x direction nearly disappears. If a particle is placed near the line of obstacles in the absence of a driving force, the particle moves at a constant velocity parallel to the line of obstacles due to the Magnus force.

If we place the particle near the line of obstacles and subject it to an ac driving force given by $F^{AC} = A\cos(\omega t)\hat{\mathbf{x}} + B\sin(\omega t)\hat{\mathbf{y}}$, we observe not only directed motion but a reversal in the direction of motion as a function of the ac drive amplitude, Magnus force, and dissipation. This occurs due to the fact that the ac drive induces a rotation of the particle that interacts like a gear mechanism with the periodicity of the line of obstacles. In Fig. 13(a) we plot the trajectory of a particle with $\alpha_m = 2.0$, $A = B = 0.05$, and $\omega = 0.00005$ which is

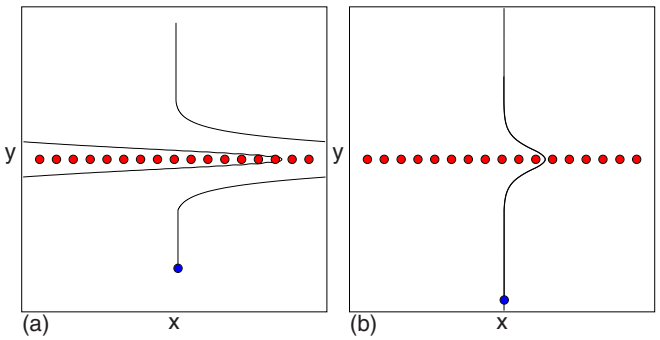

FIG. 12. The particle position (blue dot) and trajectory (line) along with the obstacle positions (red dots) for a particle with $\alpha_m = 2.0$ moving toward a line of repulsive obstacles. (a) At $F_D = 0.007$, the particle trajectory deviates into the positive x direction as it approaches the line of obstacles. (b) At $F_D = 0.07$, the x-direction deviation is smaller.

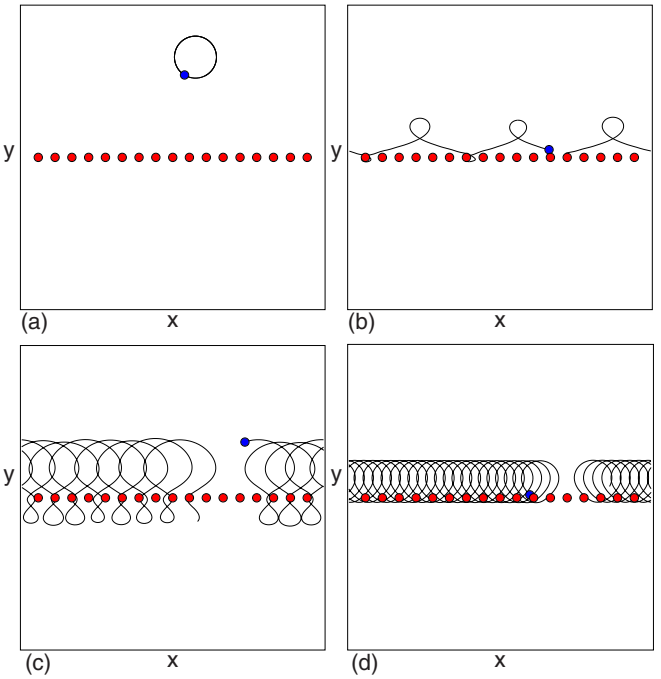

FIG. 13. The particle position (blue dot) and trajectory (line) along with the obstacle positions (red dots) for a particle interacting with a line of obstacles while subjected to an ac drive in the x and y directions. (a) A particle with $A = B = 0.05$, $\omega = 0.00005$, and $\alpha_m = 2.0$ placed at $R = 12a$, where there is no directed motion. (b) The same as panel (a) but with the particle placed at $R = 2a$, where now directed motion occurs in the positive x direction. (c) The same as panel (b) but with $A = B = 0.1$, where the directed motion is in the negative x direction. (d) The same as panel (b) but with $\alpha_m = 10$, where the directed motion is in the positive x direction.

placed at distance of $R = 12a$ from the line of obstacles. This is sufficiently far away that there is no interaction between the particle and the obstacles, and the particle executes a circular counterclockwise orbit with no directed motion. In Fig. 13(b) we keep everything the same but place the particle a distance $R = 2.0a$ from the line of obstacles. The particle now translates in the positive x direction and passes an integer number of obstacles during each ac drive cycle. In Fig. 13(c) the same system with $A = B = 0.1$ has a larger particle orbit and the particle translates in the negative x direction, indicating a reversal of the current. The effectiveness of the reversed ratchet effect is much lower, with the particle translating at 1/4 the speed of its motion in the positive x direction in Fig. 13(b). In Fig. 13(d) we show the system from Fig. 13(b) with a much larger value of $\alpha_m = 10$. The particle translates in the positive x direction but at a much smaller velocity.

In Fig. 14(a) we plot $\langle V_x\rangle$ versus A for the system in Figs. 13(b) and 13(c) with $B = A$. There is a reversal in the current from positive to negative at $A = 0.7$, while at higher A, $\langle V_x\rangle$ goes to zero. As A approaches zero, the particle moves in a straight line along the x direction at fixed $\langle V_x\rangle = 0.056$ due to the Magnus force created by the repulsion from the line of obstacles. Figure 14(b) shows $\langle V_x\rangle$ versus α_m for the system in Fig. 13(b) at fixed $A = 0.05$. For $\alpha_m < 1.5$, the particle moves in the negative x direction, while the motion is in the positive x direction when $\alpha_m \geqslant 1.5$. The efficiency of the ratchet as

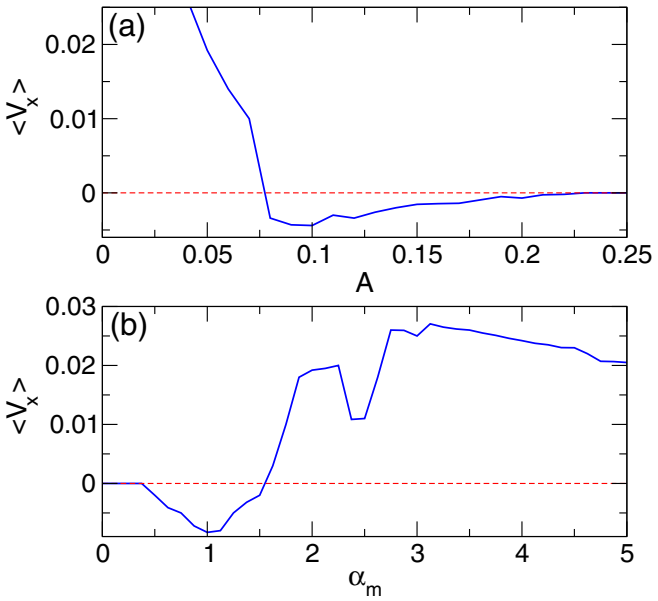

FIG. 14. (a) $\langle V_x \rangle$ vs A for the system in Fig. 13(b,c) showing a current reversal. (b) $\langle V_x \rangle$ vs α_m for the system in Fig. 13(b) with $A = 0.05$, showing a current reversal.

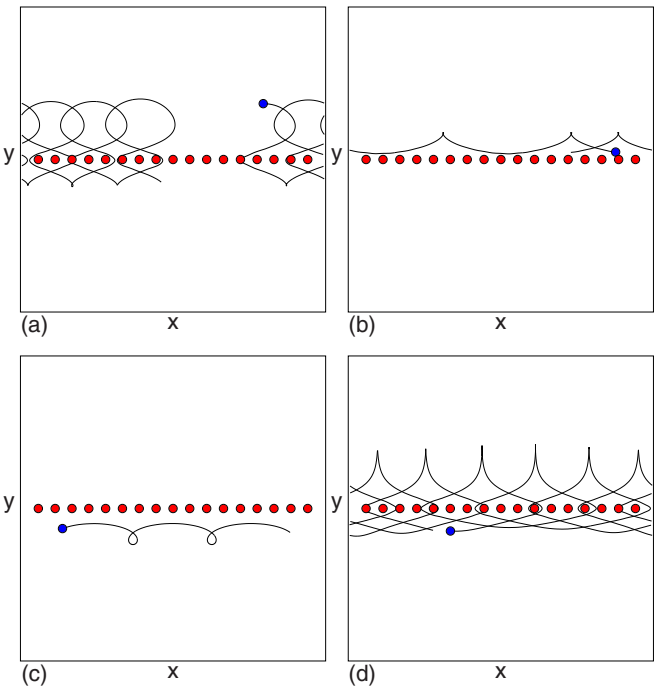

FIG. 15. The particle position (blue dot) and trajectory (line) along with the obstacle positions (red dots) for a particle interacting with a line of obstacles under an ac drive with $A = B$ and $\omega = 0.00005$. (a) The system in Fig. 14(b) with $A = B = 0.05$ at $\alpha_m = 1.0$ showing translation in the negative x direction. (b) A translating orbit with $A = B = 0.025$ where the particle does not encircle any obstacles. (c) The same as in (b) but with the particle initially placed below the line of obstacles, which produces translation in the negative x direction. (d) The system from Fig. 13(b) with only one direction of ac drive, achieved by setting $A = 0.05$ and $B = 0.0$. The ratchet effect operates at only half the velocity found for simultaneous x and y driving with $A = B = 0.05$.

measured by the magnitude of $\langle V_x \rangle$ reaches a maximum near $\alpha_m = 3.0$ and then gradually decreases with increasing α_m. The step near $\alpha_m = 2.5$ is produced by a change in the nature of the translating orbit. In Fig. 15(a) we plot the trajectory of a particle moving in the negative x direction for the system in Fig. 14(b) at $\alpha_m = 1.0$. For smaller α_m, the orbit increases in extent and the particle encircles up to three obstacles per ac drive cycle. The magnitude and direction of the rectified current depend on the starting position of the particle relative to the line of obstacles, and there can also be translating orbits that do not encircle any obstacles in which the particle skips along the edge of the line of obstacles, as shown in Figs. 15(b) and 15(c) for a particle with $A = B = 0.025$ initially placed either above or below the line of obstacles, respectively. The ratchet can also occur as function of only a single ac drive. When the ac driving force is applied only along the x direction, we find a series of ratchet effects as illustrated in Fig. 15(d) for the same system as in Fig. 13(b) but with $A = 0.05$ and $B = 0.0$. Here the particle is ratcheting in the positive direction with $\langle V_x \rangle = 0.009$, which is about half the velocity found for a ratchet effect with simultaneous x and y ac driving, $A = B = 0.05$.

The ratchet effect is strongly affected by the damping. A finite damping term causes a particle placed near a line of obstacles to move away from the obstacles gradually; however, the ac driving can maintain the ratcheting motion. In Fig. 16(a) we plot V_x versus time in simulation time steps for a particle with $\alpha_m = 2.0$ and $R = 4a$ at two different values of the damping, $\alpha_d = 0.005$ and $\alpha_d = 0.001$. For the larger damping, the particle gradually moves in the positive y direction away from the line of defects since the damping term aligns the particle velocity with the direction of the repulsive force from the defect line. In this case, as the particle moves farther away from the obstacles, the ratcheting effect is reduced. For the smaller damping, the particle oscillates

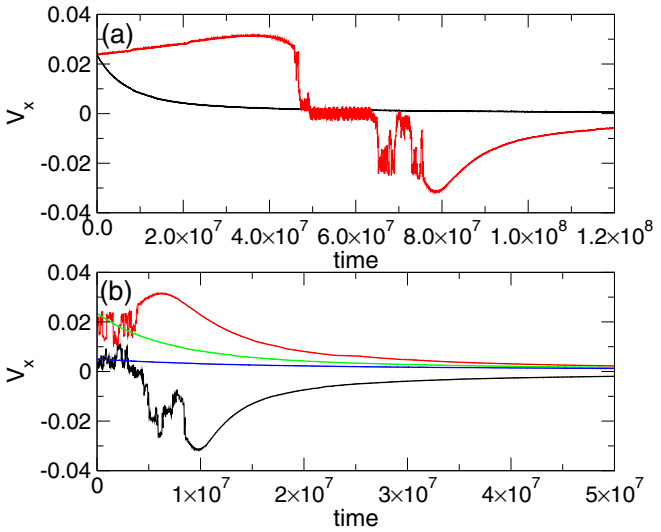

FIG. 16. (a) V_x vs time in simulation time steps for a particle with $\alpha_m = 2.0$ interacting with a line of obstacles at an initial distance of $R = 4a$ with $\alpha_d = 0.005$ (black) and $\alpha_d = 0.001$ (red). (b) V_x vs time for the same system with $\alpha_m = 2.0$ and $\alpha_d = 0.005$ for particles initialized at $R = a$ (black), $2a$ (red), $4a$ (green), and $6a$ (blue).

across the line of obstacles until it ends up below the line of obstacles and then gradually gets pushed farther away from the obstacles in the negative y direction, causing a reduction in the ratchet effect. In this case, there is also a window of time during which the particle becomes localized on an obstacle, giving a ratchet velocity of zero, while when the particle begins to spend most of its time below the line of obstacles, it begins to ratchet in the negative x direction. There are also several points at which discrete jumps occur in the velocity due to the jumping of the particle between different orbits that are commensurate with the periodicity of the obstacle line.

In Fig. 16(b) we plot V_x versus time in simulation time steps for the system in Fig. 16(a) with $\alpha_m = 2.0$ and $\alpha_d = 0.005$ for a particle placed above the line of obstacles at a distance of $R = 1a$, $2a$, $4a$, and $6a$. In this case, a particle initially placed at $R = a$ ends up below the line of obstacles and is gradually pushed farther in the negative y direction while V_x approaches zero. For $R = 2a$, the particle gradually moves away in the positive y direction but the system passes through a series of different types of orbits that ratchet in the positive x direction, as indicated by the oscillations in V_x, and there is even a peak in the velocity before it dies away to zero. For $R = 4a$, the particle enters a single orbit and gradually moves away from the line of obstacles. If we place the particle even farther away, we observe the same behavior as for the $R = 4a$ sample but with even lower values of V_x, as shown for $R = 6a$.

We note that ratchet effects with biharmonic drives have been studied for skyrmions, where a Magnus effect can come into play; however, in these studies there was still a damping term, and the internal modes of the skyrmion were also important [69,70]. The ratchet effect we observe here is more closely related to ratchet effects found in colloids undergoing circular orbits while interacting with a magnetic bubble lattice, where the asymmetry necessary to produce the ratchet arises from the ac drive and the transport occurs due to a commensuration effect with the underlying substrate [69,71,72].

C. Dynamics of clusters

We next consider the case of three or more particles. In Fig. 17 we show some representative examples of possible multiparticle orbits. For $N = 3$ particles with $\alpha_m^1 = \alpha_m^2 = \alpha_m^3 = 1.0$ that are initially placed in a row along the x direction spaced $2a$ apart, Fig. 17(a) shows the formation of a spiraling pattern, which rotates due to precession of the orbits. The particular type of orbit that appears for $N = 3$ equivalent particles depends on the initial particle placement, but in general we find nonchaotic stable orbits. In Fig. 17(b) we plot the trajectories for $N = 3$ with $\alpha_m^1 = \alpha_m^3 = 2.0$ and $\alpha_m^2 = 1.0$, where the two $\alpha_m = 2$ particles form a pair that orbits in the center of the cluster while the $\alpha_m = 1.0$ particle follows an orbit with a larger radius. An $N = 3$ sample in which all of the particles are different, with $\alpha_m^1 = 1.0$, $\alpha_m^2 = 3.0$, and $\alpha_m^3 = 2.0$, appears in Fig. 17(c). Here a layering effect occurs in which particles with larger Magnus force spend more time closer to the center of the cluster. Figure 17(d) shows the same system with $\alpha_m^1 = 1.0$, $\alpha_m^2 = 7.0$, and $\alpha_m^3 = 2.0$, where three clear spatial layers appear and the $\alpha_m = 7.0$ particle is nearest to the center. This system has some similarities to the ordering

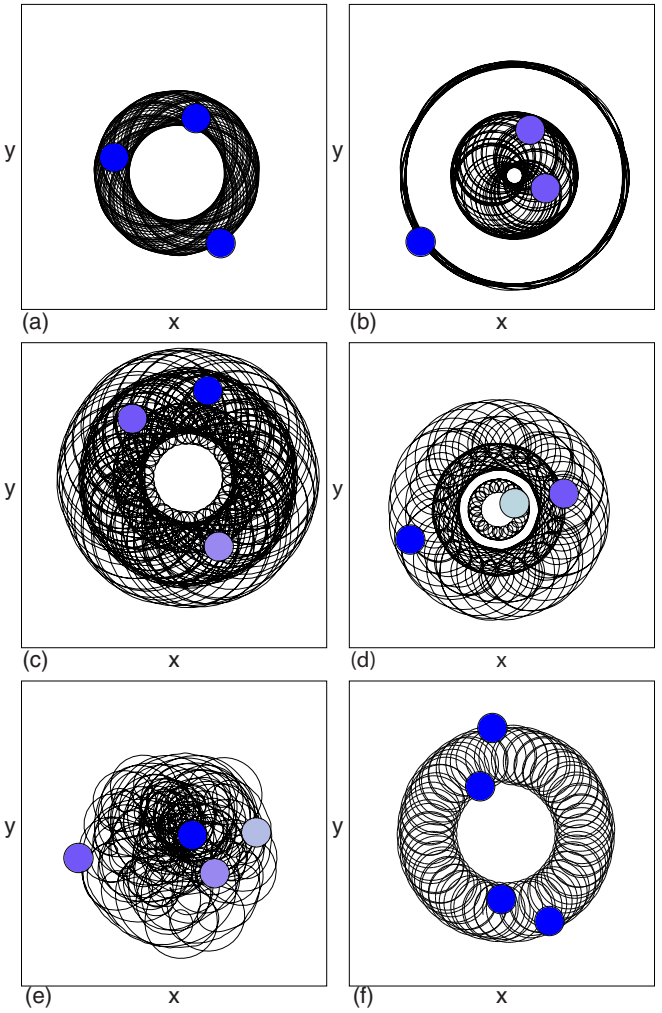

FIG. 17. The particle positions (dots) and trajectories (lines) for multiparticle systems with no drive. (a) $N = 3$, $\alpha_m^1 = \alpha_m^2 = \alpha_m^3 = 1.0$ (blue). (b) $N = 3$, $\alpha_m^1 = \alpha_m^3 = 2.0$ (blue), and $\alpha_m^2 = 1.0$ (purple). (c) $N = 3$, $\alpha_m^1 = 1.0$ (blue), $\alpha_m^2 = 3.0$ (light purple), and $\alpha_m^3 = 2.0$ (dark purple). (d) $N = 3$, $\alpha_m^1 = 1.0$ (blue), $\alpha_m^2 = 7.0$ (light blue), and $\alpha_m^3 = 2.0$ (purple). (e) $N = 4$, $\alpha_m^1 = 1.0$ (dark blue), $\alpha_m^2 = 2.0$ (dark purple), $\alpha_m^3 = 3.0$ (medium purple), and $\alpha_m^4 = 4.0$ (light blue). (f) $N = 4$, $\alpha_m^1 = \alpha_m^2 = \alpha_m^3 = \alpha_m^4 = 2.0$ (blue).

of small clusters of colloids in a trap; however, in this case the particles are continuously undergoing motion and there is no external confining trap. In Fig. 17(e) we plot the trajectories for an $N = 4$ system with varied Magnus forces of $\alpha_m^1 = 1.0$, $\alpha_m^2 = 2.0$, $\alpha_m^3 = 3.0$, and $\alpha_m^4 = 4.0$, which forms a chaotic cluster. We note that if the variations in the Magnus forces are larger, ordered states can appear with ringlike structures, which we describe in the next subsection. Studies of the nonlinear dynamics of various configurations of four point vortices can be found in Refs. [24,73]. In Fig. 17(f) we show an $N = 4$ sample with $\alpha_m^1 = \alpha_m^2 = \alpha_m^3 = \alpha_m^4 = 2.0$. In this case, the particles form two rotating pairs which rotate around each other. For $N > 3$, most orbits are chaotic, but for special initial placement conditions, it is possible to stabilize different types of rotating states. In larger clusters where the particles all have the same Magnus force, the chaotic states typically

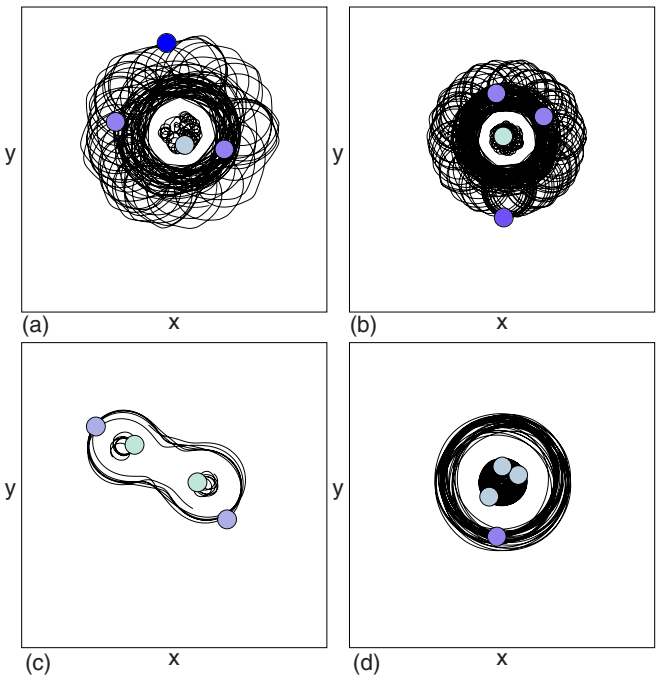

FIG. 18. The particle positions (dots) and trajectories (lines) showing ringlike structures in multiparticle systems with strong variations in the Magnus forces. (a) $N = 4$, $\alpha_m^1 = 7.0$ (light blue), $\alpha_m^2 = \alpha_m^3 = 2$ (purple), and $\alpha_m^4 = 1$ (dark blue). (b) $N = 4$, $\alpha_m^1 = 10$ (light blue), $\alpha_m^2 = 1.5$ (dark purple), and $\alpha_m^3 = \alpha_m^4 = 2$ (light purple). (c) $N = 4$, $\alpha_m^1 = \alpha_m^2 = 10$ (light blue), and $\alpha_m^3 = \alpha_m^4 = 3$ (light purple), showing a dumbbell structure. (d) $N = 4$, $\alpha_m^1 = \alpha_m^2 = \alpha_m^3 = 7$ (light blue), and $\alpha^4 = 2$ (purple).

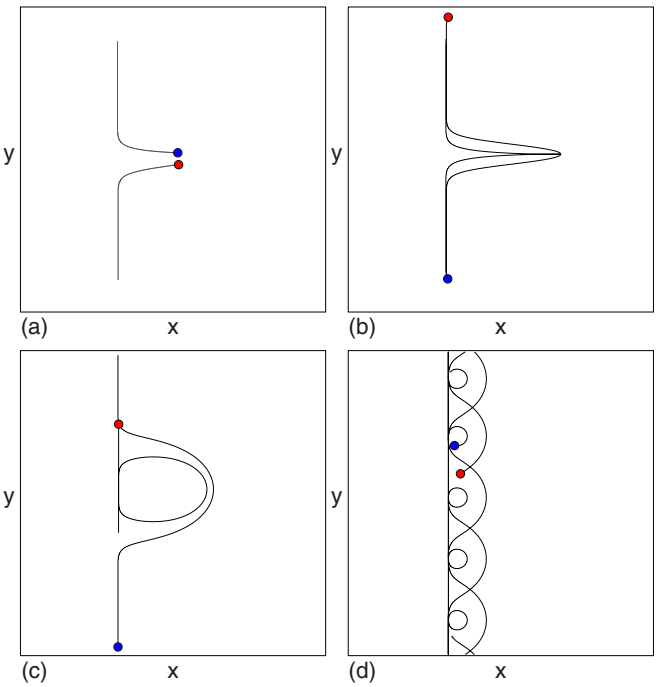

FIG. 19. (a, b) The particle positions (dots) and trajectories (lines) for two particles initialized at opposite ends of the sample under a driving force of $F_D = 0.075$. (a) The first portion of the collision for $\alpha_m^1 = 2.0$ and $\alpha_m^2 = -2.0$. (b) Continuation of the motion in (a) after the particles have passed one another. (c) Collision for $\alpha_m^1 = -2.0$ and $\alpha_m^2 = 1.85$. (d) Collision for $\alpha_m^1 = 2.0$ and $\alpha_m^2 = -1.0$.

involve a transient state of two- or three-particle subclusters that break up and re-form over time.

D. Clusters with strong variation in Magnus force strength and ring formation

For particles with Magnus forces that are of the same sign but that have sufficiently different strengths, clusters appear that have well defined spacings between the particle orbits, with the particles that have the highest Magnus force localized at the center of the cluster. In Fig. 18(a) we plot the trajectories in an $N = 4$ system with $\alpha_m^1 = 7.0$, $\alpha_m^2 = \alpha_m^3 = 2.0$, and $\alpha_m^4 = 1.0$. The $\alpha_m = 7.0$ particle becomes localized at the center of the cluster and is surrounded by a ring containing the $\alpha_m = 2.0$ particles, while the $\alpha_m = 1.0$ particle jumps between the $\alpha_m = 2.0$ ring and a partially formed outer ring. A similar structure appears in Fig. 18(b) for an $N = 4$ system with $\alpha_m^1 = 10.0$, $\alpha_m^2 = 1.5$, and $\alpha_m^3 = \alpha_m^4 = 2.0$. Other cluster shapes can form for $N = 4$, such as the $\alpha_m^1 = \alpha_m^2 = 10.0$ and $\alpha_m^3 = \alpha_m^4 = 3.0$ system shown in Fig. 18(c) where the two inner particles with $\alpha_m = 10.0$ are orbited by the $\alpha_m = 3.0$ particles to form a dumbbell shape. Strongly segregated ring structures can also occur when $N = 4$, as illustrated in Fig. 18(d) for a sample with $\alpha_m^1 = \alpha_m^2 = \alpha_m^3 = 7$ and $\alpha_m^4 = 2$, where the inner particles have the higher Magnus force. If the difference between the Magnus forces of the particles is reduced, the ring structures are lost.

E. Clusters and collisions for particles with opposite Magnus forces

As noted earlier, if two particles with equal and opposite Magnus forces come together, they can form a dipole that translates in a straight line. If the strength of the Magnus forces are different, an arching orbit appears instead. In Figs. 19(a) and 19(b) we show the trajectories of two particles with $\alpha_m^1 = 2.0$ and $\alpha_m^2 = -2.0$ under an external driving force of $F_D = 0.0075$. The particles are initially placed at the same x position but are widely separated in y. Under the influence of the drive, the particles initially move in opposite directions, but as they approach one another, they form a pair that translates in the positive x direction, as shown in Fig. 19(a). The driving force causes the particles to move closer together and eventually pass each other as shown in Fig. 19(b). Figure 19(c) shows two particles with $\alpha_m^1 = 2.0$ and $\alpha_m^2 = -1.5$ that form a dipole which moves in an arch shape before the particles decouple again. In Fig. 19(d) a system with $\alpha_m^1 = 2.0$ and $\alpha_m^2 = -1.0$ undergoes multiple collisions due to the periodic boundary conditions, and the orbit performed during each collision has a small radius due to the large difference in the strengths of the Magnus forces. If the particles are separated in y but also have a small offset in x, they do not collide head on, which creates spiraling orbits similar to that shown in Fig. 19(b) but with asymmetric loops.

For a system of three particles in which the sign of the Magnus term of one particle is opposite from that of the other two particles, we generally observe closed periodic

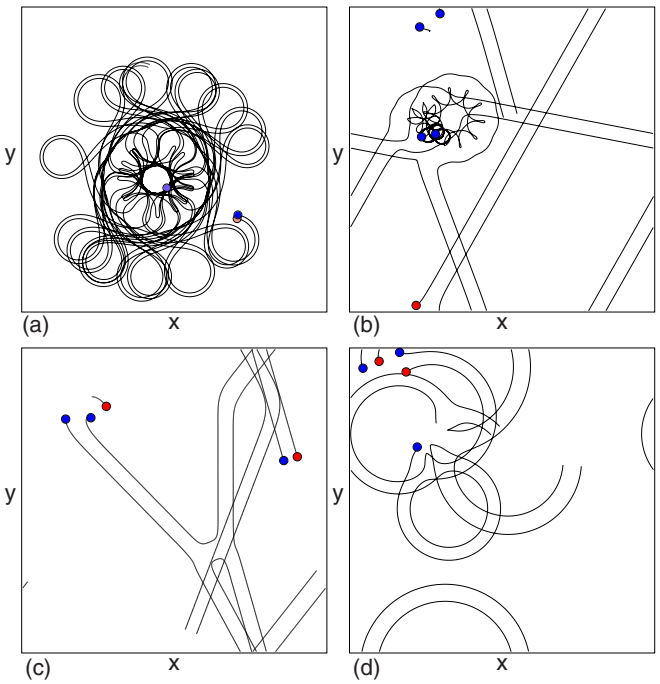

FIG. 20. The particle positions (dots) and trajectories (lines) in systems with mixed Magnus force sign and no drive. (a) A closed orbit at $N = 3$, $\alpha_m^1 = 1.0$ (purple), $\alpha_m^2 = -1.1$ (orange), and $\alpha_m^3 = 0.85$ (blue). (b) A translating dipole at $N = 5$, $\alpha_m^1 = \alpha_m^2 = \alpha_m^3 = \alpha_m^4 = 2.0$ (blue), and $\alpha_m^5 = -2.0$ (red). The two particles that are paired into the dipole are at the bottom and top of the image due to the periodic boundary conditions. (c) At $N = 5$, $\alpha_m^1 = \alpha_m^3 = \alpha_m^5 = 2.0$ (blue), and $\alpha_m^2 = \alpha_m^4 = -2.0$ (red), there are two intermittently forming pairs of dipoles. (d) Circular dipole motion at $N = 5$, $\alpha_m^1 = \alpha_m^2 = \alpha_m^5 = 2.0$ (blue), and $\alpha_m^3 = \alpha_m^4 = -1.5$ (red).

orbits; however, depending on the initial placement of the particles, it is also possible to have a pair of particles with opposite signs of Magnus force break off and move away as a dipole. In a system with mixed Magnus force amplitudes where one particle has a positive Magnus force and the other two have negative Magnus forces, a translating dipole can form that then rotates around the third particle. For example, in Fig. 20(a) a system with $\alpha_m^1 = 1.0$, $\alpha_m^2 = -1.1$, and $\alpha_m^3 = 0.85$ has a translating dipole moving in an orbit that gradually precesses counterclockwise while the third particle follows a tighter precessing orbit. For five or more particles with mixed Magnus force signs, in general we do not observe long-lived localized structures but instead find that pairs of particles with opposite sign form a gas of translating dipoles that are either broken up or deflected when a collision with another particle or dipole occurs. In Fig. 20(b) we show the trajectories of a system with five particles where $\alpha_m^1 = \alpha_m^2 = \alpha_m^3 = \alpha_m^4 = 2.0$ and $\alpha_m^5 = -2.0$. One translating dipole appears, while the other particles of the same sign form rotating clusters. When the dipole encounters a rotating cluster, it typically scatters off in a new direction after partially encircling the cluster, but there can also be an exchange of one of the dipole particles with one of the cluster particles. In Fig. 20(c) an $N = 5$ system with $\alpha_m^1 = \alpha_m^3 = \alpha_m^5 = 2.0$ and $\alpha_m^2 = \alpha_m^4 = -2.0$ has similar dynamics, but there are now two translating dipoles which undergo two types of collisions. The first is the scattering of a dipole by an isolated particle, as shown in the upper left-hand portion of the figure. The dipole can either exchange one of its particles with the isolated particle or simply be deflected. The second collision is a dipole-dipole scattering in which the dipoles can exchange particles and/or change their directions of motion. The $N = 5$ sample with $\alpha_m^1 = \alpha_m^2 = \alpha_m^5 = 2.0$ and $\alpha_m^3 = \alpha_m^4 = -1.5$ in Fig. 20(d) also contains two translating dipoles, but since the Magnus forces in the dipoles are not of equal strength, the dipole pairs move in circular paths and can break up or be deflected when they collide with each other or with the remaining stationary particle. For $N = 6$ and higher, we observe only translating and chaotic orbits. When $N = 4$, it is possible for the system to form a larger-scale translating cluster instead of a dipole, as shown in Fig. 21(a) for $\alpha_m^1 = \alpha_m^3 = 2$ and $\alpha_m^2 = \alpha_m^4 = -2$. The cluster is composed of particles that continuously switch between forming pairs of the same sign that rotate and forming pairs of the opposite sign that translate. For this combination of Magnus forces, we always observe translating clusters, but the direction and velocity of the translation depend on the initial placement of the particles. If the Magnus forces are unequal, as in Fig. 21(b) where $\alpha_m^1 = 1$, $\alpha_m^2 = \alpha_m^4 = -2$, and $\alpha^3 = 2$, similar dynamics occur but the cluster moves in a circle. Studies of the nonlinear dynamics of $N = 4$ systems composed of pairs of interacting point vortex pairs appear in Refs. [73–75].

A collection of particles with opposite Magnus force signs can be considered an example of an active matter system. In active matter, the particles are self-propelled and can be described as undergoing driven Brownian diffusion or run-and-tumble dynamics. Typically, active particles show short time ballistic behavior and long time diffusive behavior due to collisions [76,77]. In the case of the Magnus-dominated system, mixtures of opposite Magnus force signs form translating dipoles that act like active Brownian particles in the limit of zero orientational diffusion or like run-and-tumble particles with an infinite run time. When there are other particles in the system, collisions can cause the dipoles to change directions or to break up before reforming again. To highlight this effect, in Fig. 22 we plot a time series of the x-direction velocity V_x for a single particle from the system in Fig. 20(c), where regions of constant velocity are interspersed with regions of zero velocity. The constant velocity regions correspond to periods in which the particle forms half of a translating dipole, while the zero velocity regions are periods in which the particle is no longer paired into a dipole and is therefore stationary. There can also be intervals in which the particle is part of a rotating pair composed of two particles with the same Magnus force sign. In future studies, it would be interesting to examine the velocity distributions in large collections of mixtures of Magnus-dominated particles to see whether this system exhibits further similarities to active matter.

V. DISCUSSION

In Table I we provide a summary of the characteristic features associated with the different conditions considered in this work. A number of the results we observe are similar to behavior found in point vortex models. In these models, vortices in fluids are represented as nondissipative point particles

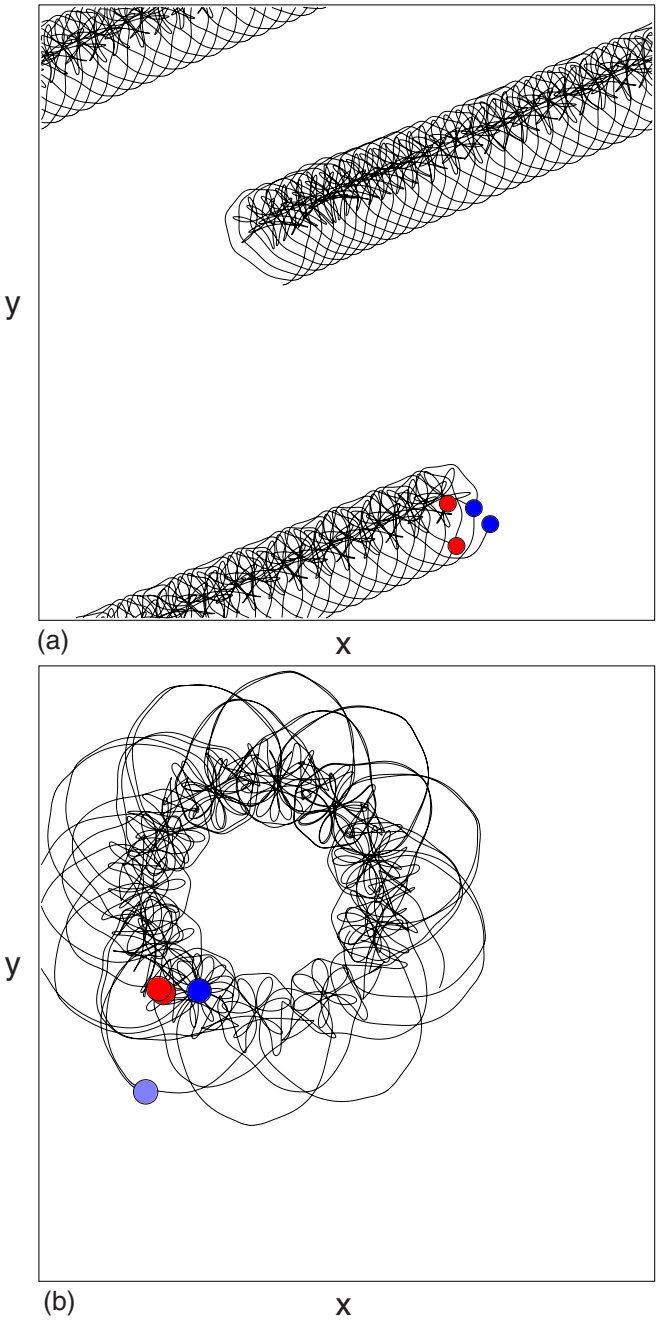

FIG. 21. The particle positions (dots) and trajectories (lines) in systems with mixed Magnus force sign and no drive. (a) For $N = 4$, $\alpha_m^1 = \alpha_m^3 = 2.0$ (blue), and $\alpha_m^2 = \alpha_m^4 = -4.0$ (red), the particles form a translating cluster. (b) For $N = 4$, $\alpha_m^1 = 1.0$ (blue), $\alpha_m^2 = \alpha_m^4 = -2$ (red), and $\alpha_m^3 = 2$ (purple), the cluster moves in a circle.

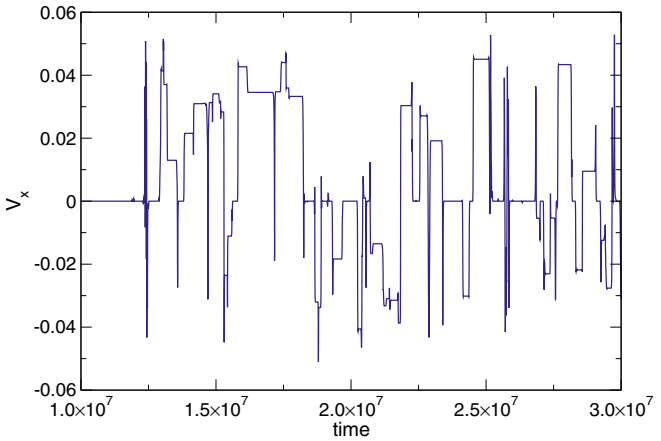

FIG. 22. The velocity component V_x vs time in simulation time steps for one of the particles in Fig. 20(c) showing jumps between zero velocity when the particle is not part of a dipole and finite velocity when the particle is part of a translating dipole.

with a logarithmic long-range interaction and nondissipative dynamics that are controlled by a Coriolis or Magnus term [23–26]. A pair of point vortices with the same vorticity rotate around one another, while a pair with opposite vorticity translate. Additionally, the point vortex literature shows that clusters of four or more particles generally form chaotic states. Other work has shown that point vortex particles can effectively be trapped in orbits around defects such as a fixed point vortex [56,78], or they can scatter off defects. In our case, the interactions are shorter range than the point vortex interactions; however, the smooth behavior of the Bessel function potential causes much of the dynamics of the Magnus-dominated particles to be fairly similar to the point vortices. In our work we considered scattering off multiple objects, ratchet effects, and particles with mixed Magnus force values. In most of the point vortex literature, the Magnus force is of the same strength, and in general, there is no driving force and dissipative effects are neglected.

Due to the dynamical nature of the states we observe, it is possible to imagine that for periodic obstacle geometries or arrangements of a large assembly of particles localized around an obstacle, some sort of dynamical but repeatable crystal could form which would be an example of a classical time crystal [79–82]. In a real system, some form of dissipation would likely arise that would eventually destroy the crystal, but it may be possible to create long-lived transient Magnus time crystals.

Experimentally, our system most closely resembles skyrmion or meron motion with no or low dissipation where the Magnus force dominates the dynamics, which should be achievable under certain conditions. Skyrmions can also be set into motion readily under a drive, so it should be possible to maintain the transient Magnus force dynamics in a low-dissipation system indefinitely by applying ac or dc driving. It is also possible to have dispersion in the Magnus force component of a skyrmion system as well as skyrmions with opposite signs. Additional internal modes can arise in skyrmions that are not taken into account in our model; however, there have already been some studies of skyrmion dynamics in the zero-dissipation limit with both Thiele equation and continuum modeling approaches [49].

Our results could also be relevant to spinning charged colloids levitated acoustically or dusty plasmas in magnetic fields, where Magnus effects arise and dissipation effects are weak. Many active spinner systems include strong dissipation or have only short-range contact interaction forces, so that two particles or a particle and an obstacle would interact only when they touch. Finally, our results for decoupling and

TABLE I. Summary of characteristic features that appear under the conditions considered in this work.

Name	Characteristic features
Two particles, no drive:	
Magnus force of same sign and strength	Stable rotating state
Magnus force of opposite sign and same strength	Stable translation in absence of drive
Two particles, with drive:	
Magnus force of same sign and strength	Stable translating state
Magnus force of same sign and different strength	Decoupling transition
With drive and obstacle:	
Low drive	Localized pinned orbit
Higher drive	Depinning transition to translating state
Multiple particles	Multiple trapping and depinning transitions possible
Multiple obstacles, funnel arrangement:	
No damping	Edge current behavior
Finite damping	Diode effect
Multiple obstacles, line arrangement:	
dc drive perpendicular to line	Deviation of motion parallel to line
Circular ac drive	Ratchet effects and ratchet reversals
Three or more particles, no drive:	
Three particles	Stable nonchaotic orbits
More than three particles	Most orbits chaotic
Strong Magnus force variation	Strongly segregated ring structures
Clusters with mixed Magnus force sign and strength:	
Equal strength, opposite sign pairs	Arching orbits
Mixed strength, mixed sign triples	Formation of translating dipole
Five or more particles	Gas of colliding translating dipoles

depinning should also be applicable to vortices and point vortex models in the presence of some form of flow field.

VI. SUMMARY

We have examined the dynamics of individual pairs and small clusters of repulsive pairwise interacting particles in which the dynamics is dominated by a Magnus term. In the overdamped limit, clusters of such particles exhibit transient motion and settle into a stationary state. For particles without dissipation, when the Magnus terms have the same strength and sign, a pair of repulsively interacting particles rotate around each other at fixed distance. Similar rotating clusters appear up to sizes of $N = 4$, but for larger clusters the dynamics become chaotic. A pair of particles with opposite Magnus force sign forms a translating dipole. Under an applied drive, an individual particle moves at 90° with respect to the drive direction, a rotating pair with the same Magnus force translates, and a pair with different Magnus force strengths have a decoupling driving force threshold. A particle interacting with repulsive obstacles forms a bound state with a critical driving threshold for the decoupling of the particle from the obstacle, while if the particle dynamics include damping, the particle gradually spirals away from the obstacle. A single obstacle can bind multiple particles simultaneously. When a rotating pair encounters a obstacle, one or both particles in the pair can become trapped. For particles interacting with clusters of obstacles, we find that it is possible for a particle to become bound to the cluster and form a circulating current around the outside of the cluster. In the overdamped limit, a particle interacting with obstacles arranged in a funnel shape exhibits a diode effect, but when there is only a Magnus force and no damping, the diode effect disappears. A line of obstacles causes a deviation in the direction of the trajectory of the driven particle, which eventually passes through the obstacle line. Under an ac drive, we show that it is possible to observe a ratchet effect for a particle placed near a line of obstacles due to a gearlike mechanism in which the particle orbit becomes commensurate with the periodicity of the obstacle line. The ratchet effect shows a reversal as a function of ac drive, Magnus force, and distance from the obstacle line. For large clusters of particles, we find that if the dispersion in the Magnus force is sufficiently large, the particles with the largest Magnus force become localized in the center of the cluster. In mixtures of particles with opposite signs, we find the intermittent formation of dipoles that can translate over some distance before breaking up or deflecting upon encountering other particles, and we show that these dipoles have certain similarities to active matter systems. Our results could applied to skyrmion systems in the absence of dissipation or in the low-dissipation limit, or to chiral active matter in which there is low damping or continuous driving. Our results could also be useful for understanding transient dynamics in systems with Magnus-dominated dynamics and weak damping.

ACKNOWLEDGMENTS

This work was supported by the US Department of Energy through the Los Alamos National Laboratory. Los

Alamos National Laboratory is operated by Triad National Security, LLC, for the National Nuclear Security Administration of the US Department of Energy (Contract No. 892333218NCA000001).

[1] R. Bubeck, C. Bechinger, S. Neser, and P. Leiderer, Melting and Reentrant Freezing of Two-Dimensional Colloidal Crystals in Confined Geometry, Phys. Rev. Lett. **82**, 3364 (1999).

[2] J. A. Drocco, C. J. Olson Reichhardt, C. Reichhardt, and B. Jankó, Structure and melting of two-species charged clusters in a parabolic trap, Phys. Rev. E **68**, 060401(R) (2003).

[3] R. W. Perry, M. C. Holmes-Cerfon, M. P. Brenner, and V. N. Manoharan, Two-Dimensional Clusters of Colloidal Spheres: Ground States, Excited States, and Structural Rearrangements, Phys. Rev. Lett. **114**, 228301 (2015).

[4] V. M. Bedanov and F. M. Peeters, Ordering and phase transitions of charged particles in a classical finite two-dimensional system, Phys. Rev. B **49**, 2667 (1994).

[5] K. Nelissen, A. Matulis, B. Partoens, M. Kong, and F. M. Peeters, Spectrum of classical two-dimensional Coulomb clusters, Phys. Rev. E **73**, 016607 (2006).

[6] L. R. E. Cabral, B. J. Baelus, and F. M. Peeters, From vortex molecules to the Abrikosov lattice in thin mesoscopic superconducting disks, Phys. Rev. B **70**, 144523 (2004).

[7] L. Komendová, M. V. Milošević, and F. M. Peeters, Soft vortex matter in a type-I/type-II superconducting bilayer, Phys. Rev. B **88**, 094515 (2013).

[8] W.-T. Juan, Z.-H. Huang, J.-W. Hsu, Y.-J. Lai, and Lin I, Observation of dust Coulomb clusters in a plasma trap, Phys. Rev. E **58**, R6947 (1998).

[9] D. Bhattacharya, A. V. Filinov, A. Ghosal, and M. Bonitz, Role of confinements on the melting of Wigner molecules in quantum dots, Eur. Phys. J. B **89**, 60 (2016).

[10] S. W. Seo, B. Ko, J. H. Kim, and Y. Shin, Observation of vortex-antivortex pairing in decaying 2D turbulence of a superfluid gas, Sci. Rep. **7**, 4587 (2017).

[11] G. Gauthier, M. T. Reeves, X. Yu, A. S. Bradley, M. A. Baker, T. A. Bell, H. Rubinsztein-Dunlop, M. J. Davis, and T. W. Neely, Giant vortex clusters in a two-dimensional quantum fluid, Science **364**, 1264 (2019).

[12] X. Zhao, C. Jin, C. Wang, H. Du, J. Zang, M. Tian, R. Che, and Y. Zhang, Direct imaging of magnetic field-driven transitions of skyrmion cluster states in FeGe nanodisks, Proc. Natl. Acad. Sci. USA **113**, 4918 (2016).

[13] A. F. Schaeffer, L. Rozsa, J. Berakdar, E. Y. Vedmedenko, and R. Wiesendanger, Stochastic dynamics and pattern formation of geometrically confined skyrmions, Commun. Phys. **2**, 72 (2019).

[14] M. X. Lim, A. Souslov, V. Vitelli, and H. M. Jaeger, Cluster formation by acoustic forces and active fluctuations in levitated granular matter, Nat. Phys. **15**, 460 (2019).

[15] F. Schmidt, B. Liebchen, H. Löwen, and G. Volpe, Light-controlled assembly of active colloidal molecules, J. Chem. Phys. **150**, 094905 (2019).

[16] L. Q. Costa Campos, S. W. S. Apolinario, and H. Löwen, Structural ordering of trapped colloids with competing interactions, Phys. Rev. E **88**, 042313 (2013).

[17] C. J. Olson Reichhardt, C. Reichhardt, and A. R. Bishop, Structure and fragmentation in colloidal artificial molecules and nuclei, Eur. Phys. J. E **22**, 11 (2007).

[18] R. Niu, T. Palberg, and T. Speck, Self-Assembly of Colloidal Molecules Due to Self-Generated Flow, Phys. Rev. Lett. **119**, 028001 (2017).

[19] H. Abdi, R. Soheilian, R. M. Erb, and C. E. Maloney, Paramagnetic colloids: Chaotic routes to clusters and molecules, Phys. Rev. E **97**, 032601 (2018).

[20] A. Aubret, M. Youssef, S. Sacanna, and J. Palacci, Targeted assembly and synchronization of self-spinning microgears, Nat. Phys. **14**, 1114 (2018).

[21] I. Williams, E. C. Oğuz, T. Speck, P. Bartlett, H. Löwen, and C. P. Royall, Transmission of torque at the nanoscale, Nat. Phys. **12**, 98 (2016).

[22] C. Reichhardt and C. J. Olson Reichhardt, Depinning and nonequilibrium dynamic phases of particle assemblies driven over random and ordered substrates: A review, Rep. Prog. Phys. **80**, 026501 (2017).

[23] H. Aref, J. B. Kadtke, I. Zawadzki, L. J. Campbell, and B. Eckhardt, Point vortex dynamics: Recent results and open problems, Fluid Dyn. Res. **3**, 63 (1988).

[24] S. Boatto and R. T. Pierrehumbert, Dynamics of a passive tracer in a velocity field of four identical point vortices, J. Fluid Mech. **394**, 137 (1999).

[25] H. Aref, Point vortex dynamics: A classical mathematics playground, J. Math. Phys. **48**, 065401 (2007).

[26] J. N. Reinaud, K. V. Koshel, and E. A. Ryzhov, Entrapping of a vortex pair interacting with a fixed point vortex revisited. II. Finite size vortices and the effect of deformation, Phys. Fluids **30**, 096604 (2018).

[27] B. A. Grzybowski, X. Jiang, H. A. Stone, and G. M. Whitesides, Dynamic, self-assembled aggregates of magnetized, millimeter-sized objects rotating at the liquid-air interface: Macroscopic, two-dimensional classical artificial atoms and molecules, Phys. Rev. E **64**, 011603 (2001).

[28] E. Climent, K. Yeo, M. R. Maxey, and G. E. Karniadakis, Dynamic self-assembly of spinning particles, J. Fluids Eng. Trans. ASME **129**, 379 (2007).

[29] D. Banerjee, A. Souslov, A. G. Abanov, and V. Vitelli, Odd viscosity in chiral active fluids, Nat. Commun. **8**, 1573 (2017).

[30] S. I. Denisov, T. V. Lyutyy, V. V. Reva, and A. S. Yermolenko, Temperature effects on drift of suspended single-domain particles induced by the Magnus force, Phys. Rev. E **97**, 032608 (2018).

[31] J.-B. Gorce, H. Xia, N. Francois, H. Punzmann, G. Falkovich, and M. Shats, Confinement of surface spinners in liquid metamaterials, Proc. Natl. Acad. Sci. USA **116**, 25424 (2019).

[32] O. Chepizhko and T. Franosch, Ideal circle microswimmers in crowded media, Soft Matter **15**, 452 (2019).

[33] W. Schirmacher, B. Fuchs, F. Höfling, and T. Franosch, Anomalous Magnetotransport in Disordered Structures: Classical Edge-State Percolation, Phys. Rev. Lett. **115**, 240602 (2015).

[34] S. Mühlbauer, B. Binz, F. Jonietz, C. Pfleiderer, A. Rosch, A. Neubauer, R. Georgii, and P. Böni, Skyrmion lattice in a chiral magnet, Science **323**, 915 (2009).

[35] X. Z. Yu, Y. Onose, N. Kanazawa, J. H. Park, J. H. Han, Y. Matsui, N. Nagaosa, and Y. Tokura, Real-space observation of a two-dimensional skyrmion crystal, Nature (London) **465**, 901 (2010).

[36] N. Nagaosa and Y. Tokura, Topological properties and dynamics of magnetic skyrmions, Nat. Nanotechnol. **8**, 899 (2013).

[37] Y.-H. Liu and Y.-Q. Li, A mechanism to pin skyrmions in chiral magnets, J. Phys.: Condens. Matter **25**, 076005 (2013).

[38] J. Müller and A. Rosch, Capturing of a magnetic skyrmion with a hole, Phys. Rev. B **91**, 054410 (2015).

[39] F. Büttner, C. Moutafis, M. Schneider, B. Krüger, C. M. Günther, J. Geilhufe, C. von Kor Schmising, J. Mohanty, B. Pfau, S. Schaffert *et al.*, Dynamics and inertia of skyrmionic spin structures, Nat. Phys. **11**, 225 (2015).

[40] C. Reichhardt, D. Ray, and C. J. Olson Reichhardt, Quantized transport for a skyrmion moving on a two-dimensional periodic substrate, Phys. Rev. B **91**, 104426 (2015).

[41] C. Reichhardt, D. Ray, and C. J. Olson Reichhardt, Collective Transport Properties of Driven Skyrmions with Random Disorder, Phys. Rev. Lett. **114**, 217202 (2015).

[42] B. L. Brown, U. C. Täuber, and M. Pleimling, Effect of the Magnus force on skyrmion relaxation dynamics, Phys. Rev. B **97**, 020405(R) (2018).

[43] W. Jiang, X. Zhang, G. Yu, W. Zhang, X. Wang, M. B. Jungfleisch, J. E. Pearson, X. Cheng, O. Heinonen, K. L. Wang *et al.*, Direct observation of the skyrmion Hall effect, Nat. Phys. **13**, 162 (2017).

[44] W. Legrand, D. Maccariello, N. Reyren, K. Garcia, C. Moutafis, C. Moreau-Luchaire, S. Coffin, K. Bouzehouane, V. Cros, and A. Fert, Room-temperature current-induced generation and motion of sub-100 nm skyrmions, Nano Lett. **17**, 2703 (2017).

[45] J.-V. Kim and M.-W. Yoo, Current-driven skyrmion dynamics in disordered films, Appl. Phys. Lett. **110**, 132404 (2017).

[46] K. Litzius, I. Lemesh, B. Krüger, P. Bassirian, L. Caretta, K. Richter, F. Büttner, K. Sato, O. A. Tretiakov, J. Förster *et al.*, Skyrmion Hall effect revealed by direct time-resolved x-ray microscopy, Nat. Phys. **13**, 170 (2017).

[47] R. Juge, S.-G. Je, D. de Souza Chaves, L. D. Buda-Prejbeanu, J. Peña Garcia, J. Nath, I. M. Miron, K. G. Rana, L. Aballe, M. Foerster *et al.*, Current-driven skyrmion dynamics and drive-dependent skyrmion Hall effect in an ultrathin film, Phys. Rev. Appl. **12**, 044007 (2019).

[48] K. Zeissler, S. Finizio, C. Barton, A. Huxtable, J. Massey, J. Raabe, A. V. Sadovnikov, S. A. Nikitov, R. Brearton, T. Hesjedal *et al.*, Diameter-independent skyrmion Hall angle observed in chiral magnetic multilayers, Nat. Commun. **11**, 428 (2020).

[49] J. Feilhauer, S. Saha, J. Tobik, M. Zelent, L. J. Heyderman, and M. Mruczkiewicz, Controlled motion of skyrmions in a magnetic antidot lattice, arXiv:1910.07388 (2019).

[50] S.-Z. Lin, C. Reichhardt, C. D. Batista, and A. Saxena, Particle model for skyrmions in metallic chiral magnets: Dynamics, pinning, and creep, Phys. Rev. B **87**, 214419 (2013).

[51] J. B. Kadtke and E. A. Novikov, Chaotic capture of vortices by a moving body. I. The single point vortex case, Chaos **3**, 543 (1993).

[52] M. Budyansky, M. Uleysky, and S. Prants, Hamiltonian fractals and chaotic scattering of passive particles by a topographical vortex and an alternating current, Physica D **195**, 369 (2004).

[53] Yu. G. Izrailsky, V. F. Kozolov, and K. V. Koshel, Some specific features of chaotization of the pulsating barotropic flow over elliptic and axisymmetric sea-mounts, Phys. Fluids **16**, 3173 (2004).

[54] E. A. Ryzhov and K. V. Koshel, Interaction of a monopole vortex with an isolated topographic feature in a three-layer geophysical flow, Nonlin. Processes Geophys. **20**, 107 (2013).

[55] H. H. Luithardt, J. B. Kadtke, and G. Pedrizzetti, Chaotic capture of vortices by a moving body. II. Bound pair model, Chaos **4**, 681 (1994).

[56] E. A. Ryzhov and K. V. Koshel, Dynamics of a vortex pair interacting with a fixed point vortex, Europhys. Lett. **102**, 44004 (2013).

[57] E. A. Ryzhov and M. A. Sokolovskiy, Interaction of a two-layer vortex pair with a submerged cylindrical obstacle in a two-layer rotating fluid, Phys. Fluids **28**, 056602 (2016).

[58] B. C. van Zuiden, J. Paulose, W. T. M. Irvine, D. Bartolo, and V. Vitelli, Spatiotemporal order and emergent edge currents in active spinner materials, Proc. Natl. Acad. Sci. USA **113**, 12919 (2016).

[59] C. Reichhardt and C. J. O. Reichhardt, Reversibility, pattern formation, and edge transport in active chiral and passive disk mixtures, J. Chem. Phys. **150**, 064905 (2019).

[60] D. G. Crowdy and J. S. Marshall, The motion of a point vortex around multiple circular islands, Phys. Fluids **17**, 056602 (2005).

[61] P Reimann, Brownian motors: Noisy transport far from equilibrium, Phys. Rep. **361**, 57 (2002).

[62] C. J. O. Reichhardt and C. Reichhardt, Rectification and flux reversals for vortices interacting with triangular traps, Physica C **432**, 125 (2005).

[63] C. C. de Souza Silva, J. V. de Vondel, M. Morelle, and V. V. Moshchalkov, Controlled multiple reversals of a ratchet effect, Nature (London) **440**, 651 (2006).

[64] Q. Lu, C. J. Olson Reichhardt, and C. Reichhardt, Reversible vortex ratchet effects and ordering in superconductors with simple asymmetric potential arrays, Phys. Rev. B **75**, 054502 (2007).

[65] N. S. Lin, T. W. Heitmann, K. Yu, B. L. T. Plourde, and V. R. Misko, Rectification of vortex motion in a circular ratchet channel, Phys. Rev. B **84**, 144511 (2011).

[66] D. Perez de Lara, M. Erekhinsky, E. M. Gonzalez, Y. J. Rosen, I. K. Schuller, and J. L. Vicent, Vortex ratchet reversal: Role of interstitial vortices, Phys. Rev. B **83**, 174507 (2011).

[67] C. Reichhardt, D. Ray, and C. J. Olson Reichhardt, Magnus-induced ratchet effects for skyrmions interacting with asymmetric substrates, New J. Phys. **17**, 073034 (2015).

[68] X. Ma, C. J. Olson Reichhardt, and C. Reichhardt, Reversible vector ratchets for skyrmion systems, Phys. Rev. B **95**, 104401 (2017).

[69] W. Chen, L. Liu, Y. Ji, and Y. Zheng, Skyrmion ratchet effect driven by a biharmonic force, Phys. Rev. B **99**, 064431 (2019).

[70] W. Chen, L. Liu, and Y. Zheng, Ultrafast ratchet dynamics of skyrmion by defect engineering under time-asymmetric magnetic fields, arXiv:2002.08865 (2020).

[71] P. Tierno, T. H. Johansen, and T. M. Fischer, Localized and Delocalized Motion of Colloidal Particles on a Magnetic Bubble Lattice, Phys. Rev. Lett. **99**, 038303 (2007).

[72] J. Loehr, D. de las Heras, A. Jarosz, M. Urbaniak, F. Stobiecki, A. Tomita, R. Huhnstock, I. Koch, A. Ehresmann, D. Holzinger, and T. M. Fischer, Colloidal topological insulators, Commun. Phys. **1**, 4 (2018).

[73] H. Aref and M. A. Stremler, Four-vortex motion with zero total circulation and impulse, Phys. Fluids **11**, 3704 (1999).

[74] B. Eckhardt and H. Aref, Integrable and chaotic motions of four vortices. II. Collision dynamics of vortex pairs, Phil. Trans. R. Soc. Lond. A **326**, 655 (1988).

[75] T. Price, Chaotic scattering of two identical point vortex pairs, Phys. Fluids A **5**, 2479 (1993).

[76] M. C. Marchetti, J. F. Joanny, S. Ramaswamy, T. B. Liverpool, J. Prost, M. Rao, and R. A. Simha, Hydrodynamics of soft active matter, Rev. Mod. Phys. **85**, 1143 (2013).

[77] C. Bechinger, R. Di Leonardo, H. Löwen, C. Reichhardt, G. Volpe, and G. Volpe, Active particles in complex and crowded environments, Rev. Mod. Phys. **88**, 045006 (2016).

[78] K. V. Koshel, J. N. Reinaud, G. Riccardi, and E. A. Ryzhov, Entrapping of a vortex pair interacting with a fixed point vortex revisited. I. Point vortices, Phys. Fluids **30**, 096603 (2018).

[79] A. Shapere and F. Wilczek, Classical Time Crystals, Phys. Rev. Lett. **109**, 160402 (2012).

[80] T. L. Heugel, M. Oscity, A. Eichler, O. Zilberberg, and R. Chitra, Classical Many-Body Time Crystals, Phys. Rev. Lett. **123**, 124301 (2019).

[81] N. Y. Yao, C. Nayak, L. Balents, and M. P. Zaletel, Classical discrete time crystals, Nat. Phys. **16**, 438 (2020).

[82] A. Libál, T. Balázs, C. Reichhardt, and C. J. O. Reichhardt, Colloidal Dynamics on a Choreographic Time Crystal, Phys. Rev. Lett. **124**, 208004 (2020).